frontiers in Drug Discovery

TYPE Original Research
PUBLISHED 12 June 2026
DOI 10.3389/fddsv.2026.1774061

OPEN ACCESS

EDITED BY
Alvaro Macias,
Spanish National Centre for Cardiovascular Research, Spain

REVIEWED BY
Eric N Jimenez-Vazquez,
University of Michigan, United States
Qadeer Aziz,
Queen Mary University of London, United Kingdom

*CORRESPONDENCE
Ilaria Rivolta,
ilaria.rivolta@unimib.it

RECEIVED 23 December 2025
REVISED 19 May 2026
ACCEPTED 26 May 2026
PUBLISHED 12 June 2026

CITATION
Melgari D, Calamaio S, Frosio A, Prevostini R, Malacrida A, Anastasia L, Pappone C, Nicolini G, Cavaletti G and Rivolta I (2026) Electrophysiological mechanisms behind the differential cardiotoxicity of chemotherapeutic agents Bortezomib and Carfilzomib. *Front. Drug Discov.* 6:1774061. doi: 10.3389/fddsv.2026.1774061

Electrophysiological mechanisms behind the differential cardiotoxicity of chemotherapeutic agents Bortezomib and Carfilzomib

Dario Melgari[1], Serena Calamaio[2], Anthony Frosio[1], Rachele Prevostini[2], Alessio Malacrida[2,3], Luigi Anastasia[1,4], Carlo Pappone[1,4], Gabriella Nicolini[2,3,5], Guido Cavaletti[2,3,5] and Ilaria Rivolta[1,2]*

[1]IMTC Institute of Molecular and Translational Cardiology, IRCCS Policlinico San Donato, San Donato Milanese, Italy, [2]School of Medicine and Surgery, University of Milano Bicocca, Milan, Italy, [3]Experimental Neurology Unit, University of Milano Bicocca, Milan, Italy, [4]School of Medicine and Surgery, Vita Salute San Raffaele University, Milan, Italy, [5]School of Medicine and Surgery, Interuniversity Centre for the Promotion of the 3Rs Principles in Teaching and Research (Centro 3R), University of Milano Bicocca, Milan, Italy

Background and Purpose: Bortezomib and Carfilzomib are first- and second-generation proteasome inhibitors that revolutionized the treatment of multiple myelomas. Despite their efficacy, they have been associated with off-target adverse events. Carfilzomib has a high rate of cardiovascular adverse events including heart failure, hypertension, ischemic heart diseases and arrhythmias. On the other hand, Bortezomib is known to cause peripheral neuropathy but has a safer cardiac profile. The mechanism behind the differential cardiac toxicity of Bortezomib and Carfilzomib is not completely understood. Thus, we aim to investigate the chronic effect of low nanomolar concentrations of Bortezomib and Carfilzomib on the electrophysiology of human-induced pluripotent-derived cardiomyocytes.

Methods and Results: in-house differentiated human-induced pluripotent-derived cardiomyocytes were incubated with Bortezomib or Carfilzomib for 16 h. Patch-clamp experiments were conducted to record spontaneous action potentials and ionic currents. Carfilzomib affected the electrophysiology of spontaneous action potentials by altering the calcium and potassium currents, without affecting the sodium current. Bortezomib showed a milder effect on action potentials, probably due to a lack of effect on the potassium current I_{Kr} and an opposite compensatory effect on the calcium and sodium currents.

Conclusion: this study proposes a novel potential pro-arrhythmic mechanism that may contribute to elucidate the differential cardiotoxicity of Bortezomib and Carfilzomib.

KEYWORDS
Bortezomib, electrophysiology, cardiomyocytes, cardio-oncology, cardiotoxicity, Carfilzomib, chemotherapy, hERG

1 Introduction

Cardio-oncology is a relatively young but rapidly expanding transdisciplinary field that addresses the complex interplay between cancer and cardiovascular disease (CVD), the two leading causes of mortality worldwide (GBD, 2017 Causes of Death Collaborators, 2018). Initially developed to investigate cardiovascular toxicity induced by anticancer therapies—commonly referred to as cancer therapy–related cardiovascular toxicity (CTR-CVT)—the field has evolved substantially over the past decade. Accumulating evidence now indicates that the relationship between cancer and cardiovascular dysfunction is bidirectional. Beyond the well-established cardiotoxic effects of cancer therapies, heart failure itself has been shown to actively promote tumor growth and progression, giving rise to the concept of reverse cardio-oncology (Caller et al., 2025; Meijers et al., 2026). Nevertheless, forward cardio-oncology remains focused on elucidating mechanisms of therapy-induced cardiovascular complications and on developing strategies to prevent or mitigate these adverse effects while preserving oncological efficacy.

Proteasome inhibitors (PIs) represented a cornerstone in the treatment of multiple myelomas (MM). By inhibiting the ubiquitin protein degradation pathway, PIs promote accumulation of misfolded proteins in the endoplasmic reticulum of MM cells, ultimately inducing cell stress and apoptosis (Ito, 2020). Bortezomib (BTZ) was the first PI approved in 2003, revolutionizing MM therapy and significantly improving patient survival. BTZ acts a reversible inhibitor of the 20S proteasome, but, despite its efficacy, it is frequently associated with dose-limiting peripheral neuropathy that can cause also premature chemotherapy discontinuation (Schlafer et al., 2017). Carfilzomib (CFZ) is a second-generation PI that was developed and approved to overcome resistance and reduce the neurological side effects observed with BTZ (Kortuem and Stewart, 2013). CFZ irreversibly binds the 20S proteasome with higher potency and greater selectivity when compared to BTZ (Wu et al., 2020), resulting in improved antimyeloma efficacy. Despite their clinical success, PIs have been associated with some degree of cardiovascular toxicity, with marked differences between BTZ and CFZ. BTZ has a relatively low reported incidence of CTR-CVT, estimated at approximately 1%–4% (Meijers et al., 2026), and is only rarely associated with cardiac adverse events such as heart failure, atrial fibrillation, or bradyarrhythmia (Diwadkar et al., 2016; Buza et al., 2017; Chen et al., 2017). In contrast, CFZ consistently exhibits a substantially higher risk of adverse cardiovascular events (ACVEs), including hypertension, heart failure, ischemic heart disease, arrhythmias, and cardiac death, with reported incidence rates reaching up to 25% in clinical trials (Atrash et al., 2015; Georgiopoulos et al., 2023). In the phase III ENDEAVOR trial, CFZ-treated patients showed significantly higher rates of grade ≥3 heart failure and hypertension compared with BTZ-treated patients (Dimopoulos et al., 2016). Similarly, the phase III ASPIRE trial and pooled analyses of phase II studies confirmed an increased incidence of CFZ-associated cardiac events in heavily pre-treated MM patients (Siegel et al., 2013; Stewart et al., 2015). Notably, PIs are known to interfere with the electrophysiology of excitable cells by modulating ion channel expression and function (Tomita et al., 2019; So et al., 2019; Cammann et al., 2023), suggesting that electrical dysfunction may represent an early and sensitive marker of cardiotoxicity and a potential substrate for arrhythmogenesis.

Although these clinical observations are compelling, the molecular and cellular mechanisms underlying PI-induced cardiotoxicity—and, in particular, the basis for the differential cardiovascular risk between BTZ and CFZ—remain incompletely understood. Most experimental studies addressing PI cardiotoxicity have focused on high drug concentrations that induce overt cellular stress, mitochondrial dysfunction, and apoptosis (Hasinoff et al., 2017; Efentakis et al., 2019; Forghani et al., 2021; Tantawy et al., 2021). While these approaches have yielded important mechanistic insights, they do not fully reflect the chronic, low-dose exposure conditions encountered in clinical practice. Moreover, the proposed mechanisms largely rely on shared pathways of cellular damage and apoptosis, which do not adequately explain the distinct cardiotoxic profiles of BTZ and CFZ.

In this context, we adopted a forward cardio-oncology perspective and focused on a specific and well-defined aspect of cardiomyocyte physiology: electrical activity. Using human induced pluripotent stem cell–derived cardiomyocytes (hiPS-CMs), we investigated the chronic effects of clinically relevant low nanomolar concentrations of BTZ and CFZ (Malacrida et al., 2021) on spontaneous and triggered action potential properties, and underlying ionic currents. By isolating electrophysiological alterations in the absence of overt cytotoxicity, this study aims to uncover previously unrecognized mechanisms contributing to PI-associated cardiotoxicity and to provide new insight into the differential cardiac risk associated with BTZ and CFZ treatment.

2 Materials and methods

2.1 Human iPS cells culture and differentiation

A human-induced pluripotent-derived stem cells (hiPSCs) cell line from a healthy female donor (Thermo Fisher Scientific, cell line: TMOi001-A) was maintained on human Biolaminin 521 LN-coated dishes in TeSR-E8 TM medium (Thermo FisherScientific) (Calamaio et al., 2023). The PSC Cardiomyocytes Differentiation Kit (Thermo Fisher Scientific) was used for cardiac differentiation of monolayer culture on Matrigel® hESC-qualified Matrix (Corning, Corning, NY, United States) dishes. hiPSC-CMs cultures were enriched on day 21 of differentiation using the PSC-Derived Cardiomyocyte Isolation Kit (Miltenyi Biotech) and maintained until day 28 in culture in Cardiomyocytes Maintenance Medium (CMM) with B27 supplement (Thermo Fisher Scientific) (Tarantino

Abbreviations: PIs, Proteasome inhibitors; MM, multiple myeloma; BTZ, bortezomib; CFZ, carfilzomib; CONT, control; ACVEs, adverse cardiovascular events; HF, heart failure; hiPS-CMs, human induced-pluripotent-derived cardiomyocytes; TTX, tetrodotoxin; HP, holding potential; APs, action potentials; MDP, maximal diastolic potential; APA, action potential amplitude; APDX, action potential duration at X% of repolarization; dV/dt, maximal upstroke velocity; SEM, standard error of the mean; CVD, cardiovascular disease; CTR-CVT, cancer therapy-related cardiovascular toxicity; ER, endoplasmic reticulum.

et al., 2024). At least 48 h before electrophysiological experiments, hiPSC-CMs were detached, and single cells were replated on Matrigel-coated 35 mm dishes (VWR).

2.2 Drugs preparation and cell incubation

BTZ (LC Laboratories) and CFZ (AMGEN) stock solutions were prepared in DMSO and stored at −20 °C. Intermediate and final dilutions were made directly in culture medium. Final working concentrations were 3.2 nM and 2.8 nM for CFZ and BTZ respectively (vehicle final concentration below $1:10^{-6}$). Cells were incubated with either drug for 16 h. This experimental setting is considered appropriate to study the chronic effect of PIs (Zhou et al., 2023). For the study of ionic currents, stock solutions of Tetrodotoxin (TTX), nifedipine and E-4031 were prepared and stored at −20 °C. On each experimental day, stock solutions were diluted to final working concentrations directly in the recording bath solution and delivered to the cells through a gravity-driven perfusion system.

2.3 Proteasome inhibition assay

Following 16 h of incubation with BTZ, CFZ, or vehicle, cells were washed twice with PBS and lysed in 100 µL of lysis buffer (5 mM HEPES pH 7.5, 150 mM NaCl, 10% glycerol, 1% Triton X-100, 1.5 mM $MgCl_2$, 5 mM EGTA) for 30 s. Cell suspensions were mechanically scraped, collected, and clarified by centrifugation at 15,000 × g for 15 min at 4 °C. Protein concentration was determined using the Pierce BCA Protein Assay Kit (Thermo Fisher) and a Nanodrop spectrophotometer. Proteasome activity was assessed using 30 µg of total protein per well in black 96-well plates. Samples were incubated with 10 µL of 10× proteasome buffer (250 mM HEPES pH 7.5, 5 mM EDTA pH 8.0, 0.5% NP-40, 0.01% SDS) and 10 µL of the fluorogenic proteasome substrate N-Succinyl-Leu-Leu-Val-Tyr-7-amido-4-methylcoumarin (7.6 mg/mL; Sigma-Aldrich). After 2 h at 37 °C, fluorescence was measured using a microplate reader (Excitation: 380 nm; Emission: 460 nm; Varioskan™ LUX, Thermo Fisher).

2.4 Electrophysiology recordings

All electrophysiological patch-clamp experiments were performed with a 700B Axon operational amplifier (Molecular Devices, LLC). Spontaneous action potentials (APs) were recorded from single or small clusters of beating hiPSC-CMs at 37 °C using the whole-cell current-clamp configuration in gap-free mode (I = 0). Stimulated APs were recorded from single cells in whole-cell current-clamp mode. Membrane potential was adjusted to approximately −70 to −80 mV, and APs were elicited by injection of 20 ms depolarizing current pulses delivered at 0.5 Hz. Current amplitude was set to the minimum value required to reach the AP threshold. Ion currents were recorded in the same experimental setting but in voltage-clamp configuration and only on single cells. Patch-clamp glass pipettes were pulled with a P1000 horizontal puller (Sutter) to a final resistance of 5–8 MΩ for APs and 2–3 MΩ for ionic currents. Cell membrane capacitance and 60%–80% of series resistance were compensated only to record ionic currents. APs and fast ionic currents (i.e. sodium and calcium currents) were sampled at 50 kHz and low-pass filtered at 10 kHz, while slow ionic currents (i.e. potassium current) were sampled at 10 kHz and low-pass filtered at 1 kHz.

Spontaneous and stimulated APs as well as all ionic currents were recorded in the same extracellular solution containing (in mM): NaCl 140, KCl 5.4, $CaCl_2$ 1.8, $MgCl_2$ 10, HEPES 5, Glucose 10 (pH 7.4 with NaOH, 308 mOsm). For isolation of I_{CaL}, 10 µM nifedipine was added and currents were obtained by subtraction. Likewise, 30 µM TTX was used to isolate I_{Na}. Finally, I_{Kr} was derived by adding to the solution 3 µM E-4031. For APs and I_{Kr} the intracellular pipette solution was (in mM): NaCl 10, KCl 120, $CaCl_2$ 2, $MgCl_2$ 2, HEPES 10, EGTA-KOH 5, Na_2-ATP 2, Na_2-GTP 0.1, Na2-Creatine Phosphate 5 (pH 7.2 with KOH, 298 mOsm). For I_{CaL} and I_{Na} the intracellular pipette solution comprised (in mM): NaCl 10, CsCl 135, $CaCl_2$ 2, HEPES 10, EGTA 5, Mg-ATP 2, TEA-Cl 2 (pH 7.2 with CsOH, 298 mOsm).

Sodium (I_{Na}) and calcium (I_{Ca}) currents were elicited with the same voltage protocol consisting of consecutive 150 ms depolarizing steps from −80 to +60 mV in 10 mV increments from a holding potential (HP) of −80 mV. Pharmacological inhibition with TTX and nifedipine was assessed by applying a 150 ms depolarizing steps from −80 mV to −20 for I_{Na} recordings or to 0 mV for I_{Ca}. Potassium currents (I_K) were elicited by a two steps voltage protocol: from a HP of −80 mV, cells were depolarized for 2 s to test potential ranging from −40 to +50 mV in 10 mV increment. Tail currents were subsequently recorded by a second 3 s repolarizing step to −40 mV before returning to HP. Start-to-start interval was 6.5 s. E-4031inhibition was assessed using a 2 s depolarizing step to +20 mV followed by a 3 s step to −40 mV. Experiments were performed across independent differentiation batches, and the observed BTZ- and CFZ-associated effects were consistently reproduced. Similarly, APs and ionic current were recorded from separate but experimentally matched cell preparations, rather than form the same individual cells.

2.5 Real-time PCR

Real-time PCR (RT-PCR) was performed on hiPSC-CMs treated with BTZ and CFZ. Untreated hiPSC-CMs were used as negative controls (CONT). The Supplementary Materials section reports a detailed methods paragraph and primers sequence (Supplementary Table S1).

2.6 Analysis

Data were processed with Clampfit 11.2 (Molecular Devices, LLC), OriginPro 2016 (OriginLab), GraphPad Prism 9 (GraphPad Software, LLC) and Excel 2016 (Microsoft). Spontaneous APs were analyzed with the template search module of Clampfit to extrapolate the following parameters: maximal diastolic potential (MDP), firing frequency, action potential amplitude (APA), action potential duration at X% repolarization (APDX) and maximal upstroke velocity (dV/dt). Stimulated APs were analyzed with the same software to extrapolate APA, APDs and dV/dt.

For voltage dependence of channel activation, experimental data were fitted with the following Boltzmann sigmoidal equation:

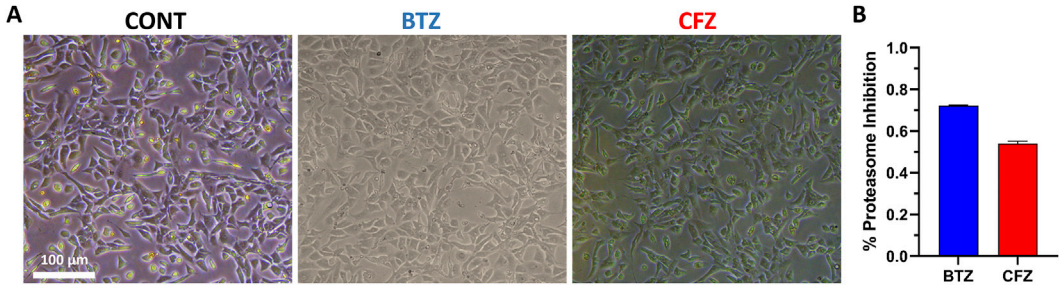

FIGURE 1
hiPS-CMs viability and proteasome inhibition assay. **(A)** Representative bright-field images of untreated hiPS-CMs (CONT) or after 16 h incubation with either BTZ or CFZ. **(B)** Proteasome inhibition levels in hiPS-CMs treated with BTZ or CFZ (N = 2).

$$y = \frac{top - bottom}{1 + e^{\left(Vm - V_{\frac{1}{2}}\right) / Slope}} + top$$

Were Vm is the membrane voltage, $V_{1/2}$ is the voltage of half-activation, top and bottom are the maximum and minimum value of the curve respectively and Slope is the slope of the curve.

2.7 Statistics

All data are presented as mean ± SEM, n indicates the number of cells and N the number of replicates (e.g. number of differentiations or experimental days). For electrophysiological data, Shapiro-Wilk normality test was used to determine data distribution. In case of normal distribution, statistical analysis was performed with ordinary 1- or 2-Way ANOVA with Donnet's *post hoc* test for multiple comparisons. Otherwise, the non-parametric Kruskal-Wallis test was used. Regarding RT-PCR data, a repeated measures One-way ANOVA test was utilized. The assumption of sphericity was formally evaluated using Mauchly's test. In instances where the assumption of sphericity was violated ($p < 0.05$), the Greenhouse-Geisser correction was applied to adjust the degrees of freedom and ensure the validity of the F-statistic. Post-hoc multiple comparisons to evaluate differences between individual treatments and the untreated control group were performed using Dunnett's test. In general, data were considered statistically significant at p values <0.05.

3 Results

3.1 Nanomolar concentrations of BTZ and CFZ inhibited the proteasome without affecting hiPS-CMs viability

hiPS-CMs were incubated at 37 °C with 2.8 nM BTZ or 3.2 nM CFZ for 16 h; these same concentrations were reported previously, although in a different model (Malacrida et al., 2021). Cell viability was not affected by the treatment as assessed by visual inspection (Figure 1A). On the other hand, the proteasome was efficiently inhibited above 50% for both BTZ and CFZ (Figure 1B). As proof of concept, higher concentrations of both compounds (e.g. 5 and 10 nM) and longer periods (24 h) of incubation were also tested on HEK293T cells causing a dramatic drop in cell viability (data not shown).

3.2 CFZ, but not BTZ, significantly altered spontaneous APs in hiPS-CMs

Incubation of hiPS-CMs with 2.8 nM BTZ for 16 h produced only minor electrophysiological changes. A non-significant trend toward prolonged spontaneous action potential durations (APDs) was observed, together with a modest reduction in maximum upstroke velocity (dV/dt). All other parameters, including spontaneous firing frequency, maximum diastolic potential (MDP), and action potential amplitude (APA), remained comparable to untreated cells. In contrast, exposure to 3.2 nM CFZ significantly affected spontaneous APs properties. In particular, CFZ depolarized the MDP and reduced both APA and dV/dt (Figure 2; Supplementary Table S2). Interestingly, a significant increase in the ratio between the action potential duration at 90% and 50% of repolarization (APD90/APD50) was also observed (Figure 2G). This seemed to reflect a tendency of CFZ in reducing the AP early phase while prolonging the final portions of repolarization, as also shown in Figure 2F. Finally, no significant effect was observed on the spontaneous APs firing frequency.

The electrophysiological changes due to CFZ treatment were reflected in the distribution of hiPS-CMs subpopulations. These were assessed using two literature-based methods. First, we applied the classification proposed by Ma and colleagues (Ma et al., 2011) in which cells were categorized as ventricular- or atrial-like based on the (APD30-APD40)/(APD70-APD80) ratio ("Method 1" in Figure 3A). Cells with a ratio above 1.5 were classified as ventricular-like, whereas cells with a ratio below 1.5 were classified as atrial-like. Using this approach, untreated cultures consisted of 59% ventricular-like cells (47/80) and 41% atrial-like (33/80). Similar proportion was observed after BTZ treatment, with 63% ventricular-like (47/75) and 37% atrial-like cells (28/75). In contrast, the treatment with CFZ significantly shifted this distribution, reducing ventricular-like cells to 25% (19/77) and increasing atrial-like cells to 75% (58/77). To further characterized the hiPS-CMs subpopulations, we also applied a more stringent classification method ("Method 2" Figure 3B) based on criteria described by Burridge (Burridge et al., 2014). Ventricular-like cells were defined by MDP < −50 mV, dV/dt > 10, APA >90 mV, and APD90/APD50 < 1.4. Atrial-like cells met the same criteria but showed an APD90/APD50 ratio >1.7. Nodal-like cells displayed a more depolarized MDP, slower dV/dt, and an APD90/APD50 ratio between 1.4 and 1.7. Cells failing to meet any

10.3389/fddsv.2026.1774061

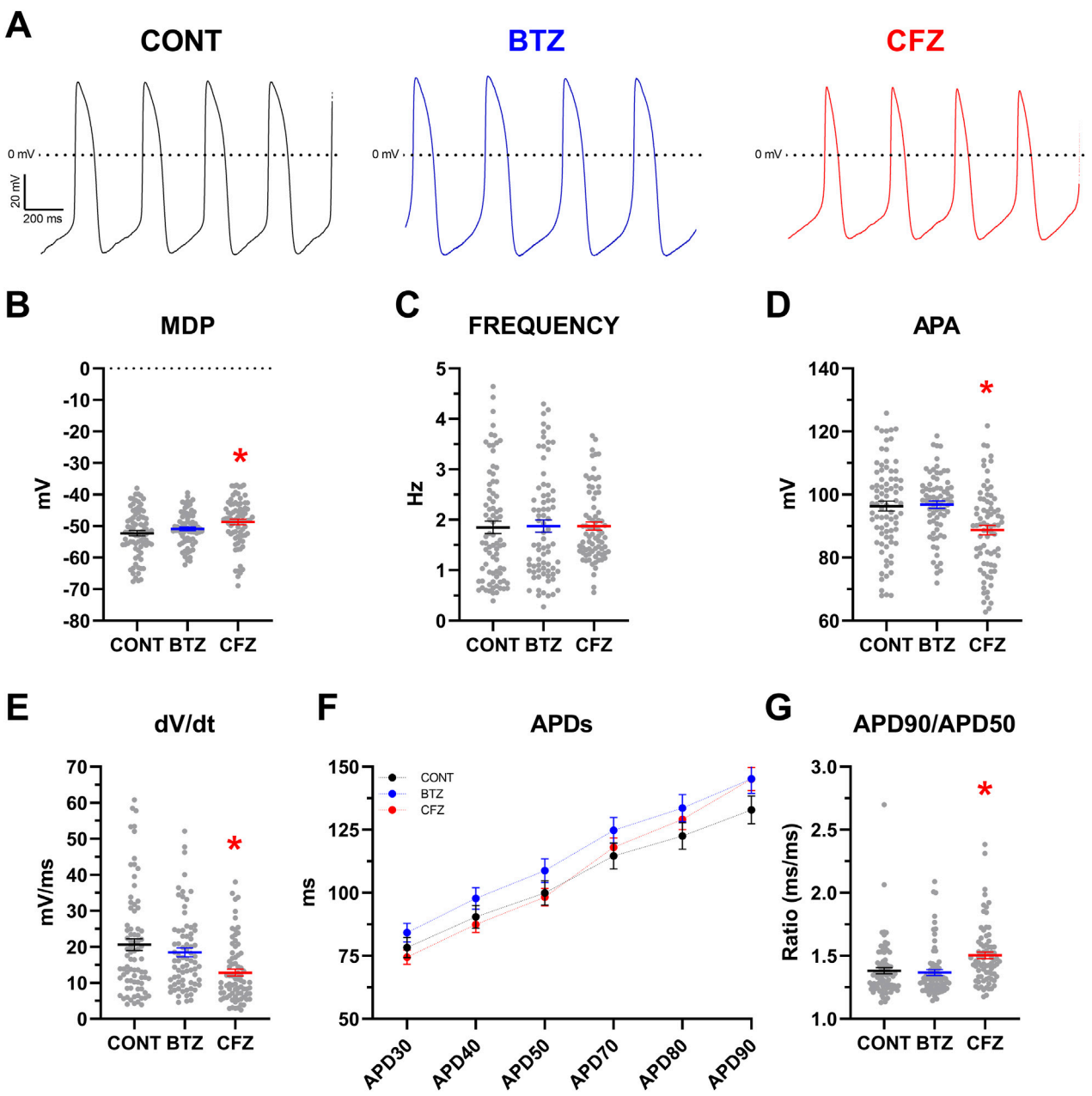

FIGURE 2
BTZ and CFZ effects on spontaneous APs in hiPS-CMs. **(A)** Sample traces of spontaneous APs from Control untreated cells (CONT) and from cells treated either with BTZ or CFZ. Given the intrinsic variability of AP waveforms in hiPSC-CMs, the traces shown were selected as those most closely matching the mean electrophysiological profile of each experimental group. **(B–G)** Electrophysiological parameters for spontaneous APs recorded from untreated cells (CONT) or in cells treated with BTZ or CFZ. Each spot represents a single cell. Bars indicate mean ± SEM. MDP = maximum diastolic potential, APA = action potential amplitude, APDX = action potential duration at X% of repolarization, dV/dt = maximum rise slope (n = 80, 75 and 77 cells for CONT, BTZ and CFZ, respectively, from N = 9 independent differentiations. *p < 0.05 1-Way ANOVA with Dunnet's *post hoc* or Kruskal-Wallis with Dunn's *post hoc*).

criterion were excluded from the analysis. Using this method, Untreated cultures consisted of 80% ventricular-like, 20% nodal-like, and 0% atrial-like cells (32/40, 8/40, and 0/40, respectively). BTZ-treated cultures showed a similar distribution, with 90% ventricular-like, 8% nodal-like, and 2% atrial-like cells (35/39, 3/39, and 1/39, respectively). In contrast, this analytical approach further confirmed that CFZ-treated cells exhibited a lower prevalence of the ventricular-like phenotype (36%) and a prevalence of nodal-like cells (58%), while atrial-like cells accounted for 6% of the population (12/33, 19/33, and 2/33, respectively). The occurrence of pro-arrhythmic events was also evaluated, and no significant difference was observed among groups. Early-after depolarizations occurred in 3.8% of untreated cells (3/80), 2.7% of BTZ-treated cells (2/75) and 3.9% of CFZ-treated cells (3/77). Delayed-after depolarizations were detected in 31.3% of untreated cells (25/80), 33.3% of BTZ-treated cells (25/75) and

10.3389/fddsv.2026.1774061

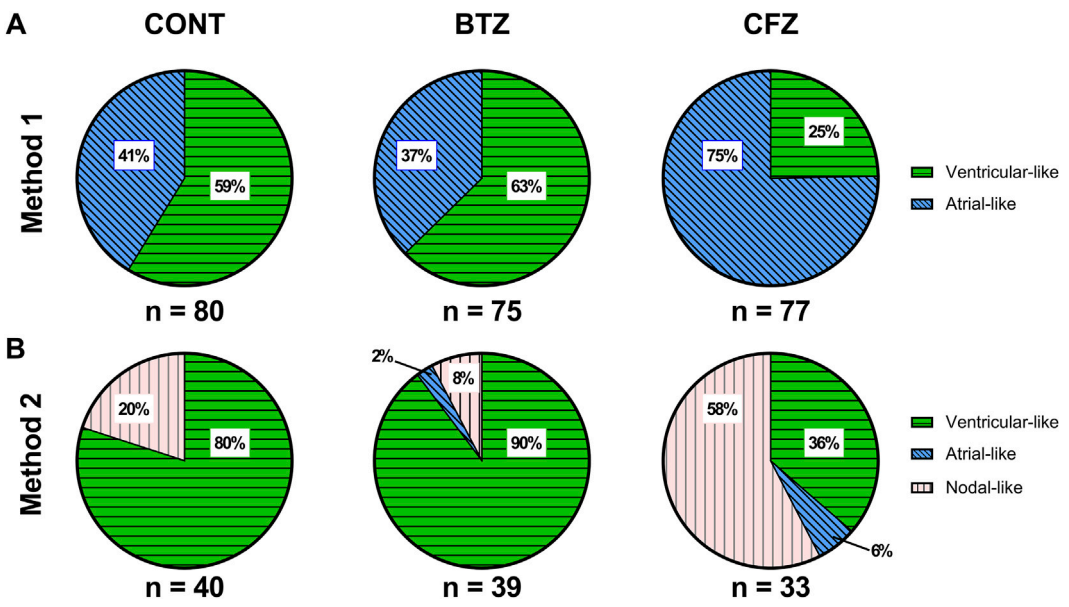

FIGURE 3
BTZ and CFZ effect on hiPS-CMs subpopulations distribution. **(A)** hiPS-CMs subpopulations distribution according to the classification method by Ma et al., 2011 (Method 1) in untreated control (CONT) and in cells treated with BTZ or CFZ. **(B)** hiPS-CMs subpopulations distribution according to the classification method by Burridge et al. (2014) (Method 2) in untreated control (CONT) and after treatment with BTZ or CFZ.

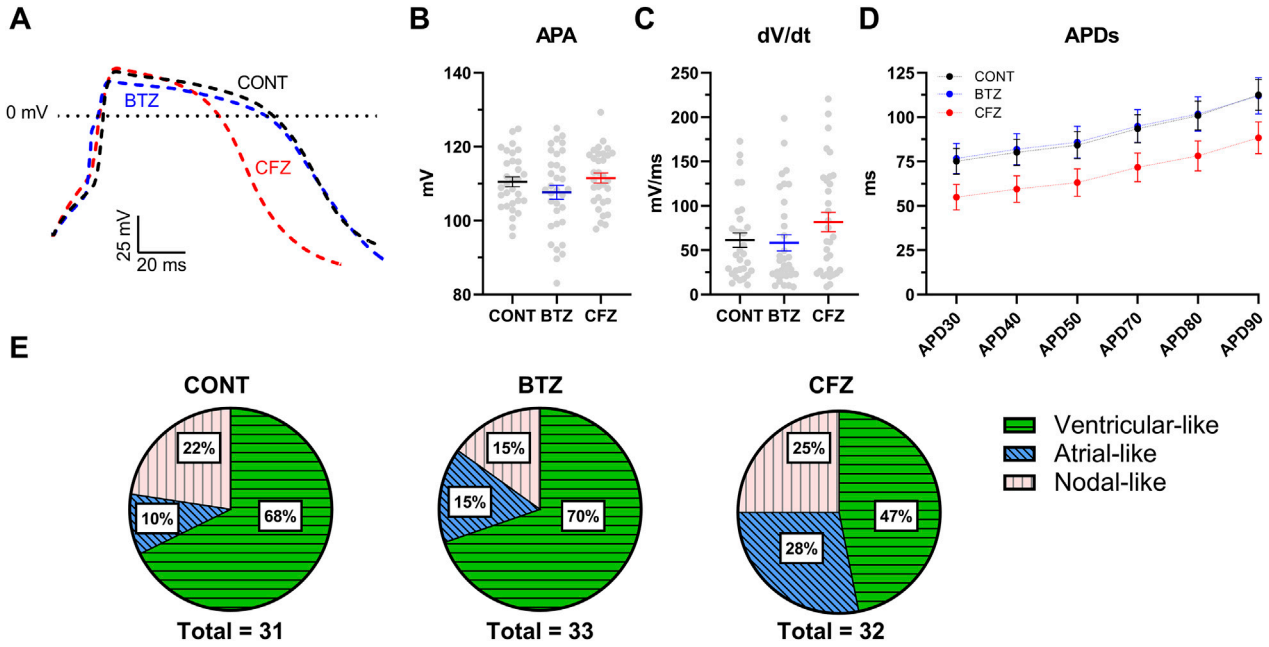

FIGURE 4
BTZ and CFZ effects on stimulated APs in hiPS-CMs. **(A)** Superimposed sample traces of averaged APs triggered at 0.5 Hz in Control (CONT, black line), BTZ (blue line), CFZ (red line). **(B–D)** Electrophysiological parameters for stimulated APs recorded from untreated cells (CONT) or in cells treated with BTZ or CFZ. Each spot represents a single cell. Bars indicate mean ± SEM. APA = action potential amplitude, dV/dt = maximum rise slope, APDX = action potential duration at X% of repolarization (*p < 0.05 1-Way ANOVA with Dunnet's *post hoc* or Kruskal-Wallis with Dunn's *post hoc*). **(E)** hiPS-CMs subpopulations distribution according to the APD90/APD50 threshold rule from Burridge et al. (2014).

32.5% of CFZ-treated cells (25/77) (not shown). Altogether, these findings indicated that CFZ, but not BTZ, significantly affected the electrophysiological profile of spontaneously beating hiPS-CMs, leading to a marked reduction in the proportion of cells displaying a clear ventricular-like electrical phenotype and favoring the nodal-like one.

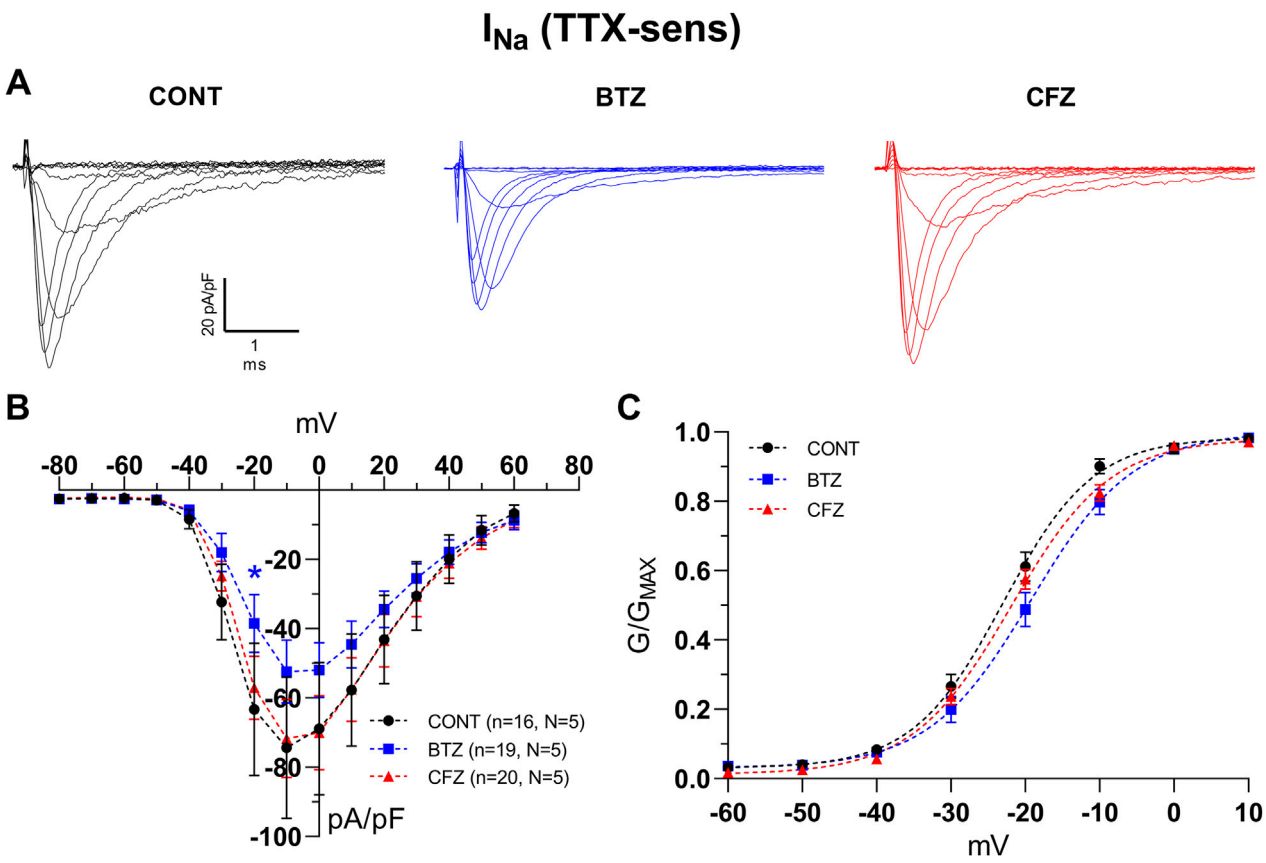

FIGURE 5
BTZ and CFZ effects on TTX-sensitive I_{Na} in hiPS-CMs. **(A)** Representative I_{Na} traces from control untreated cells (CONT) and from cells incubated with BTZ or CFZ. **(B)** Current-voltage relationship of I_{Na} in untreated cells (black circles) and after the incubation with BTZ (blue squares) or CFZ (red triangles). **(C)** Voltage dependence of channel activation of I_{Na} in control or after the incubation with BTZ and CFZ. (n = number of cells, N = number of differentiations) (*p < 0,05 2-Way ANOVA with Dunnet's *post hoc*).

3.3 BTZ and CFZ effects of stimulated APs in hiPS-CMs

To achieve a more complete electrophysiological characterization, the effect of BTZ and CFZ were also evaluated on stimulated APs in hiPS-CMs. Consistent with previous report (Koivumäki et al., 2018), paced APs showed larger APA and dV/dt values than spontaneous APs, whereas all the APDs remained within a comparable range (Figures 2, 4; Supplementary Tables S2, S3). At the stimulation frequency of 0.5 Hz, APs recorded from BTZ-treated hiPS-CMs largely overlapped with those of untreated cells (Figures 4A,D; Supplementary Table S3). In contrast, CFZ treatment produced a modest increase in dV/dt together with a reduction in all the calculated APDs (Figures 4C,D), although these changes did not reach statistical significance. These effects were also reflected in the distribution of hiPS-CM subpopulations (Figure 4E). Since the resting membrane potential was imposed experimentally and APA values were generally above 90 mV, cell classification was based exclusively on the APD90/APD50 criterion described by Burridge et al. (2014) (see previous paragraph). Using this approach, ventricular-like cells accounted for 68% (21/31) of control cells and 70% (23/33) of BTZ-treated cells. Atrial-like cells represented 10% (3/31) and 15% (5/33) of control and BTZ groups, respectively, whereas nodal-like cells accounted for 22% (7/31) and 15% (5/33). In contrast, CFZ again affected the subpopulations distribution. Only 47% (15/32) of CFZ-treated cells were classified as ventricular-like, while atrial-like and nodal-like cells represented 28% (9/32) and 25% (8/32) of the population, respectively. No relevant pro-arrhythmic events were observed under any experimental conditions. Overall, these findings further confirmed that CFZ but not BTZ affected the electrophysiological properties of hiPS-CMs. To investigate the mechanisms underlying the observed AP changes, the effects of BTZ and CFZ on the main ionic currents were subsequently evaluated.

3.4 Differential modulation of BTZ and CFZ on inward currents in hiPSC-CMs

The sodium current (I_{Na}) was assessed as the TTX-sensitive component of the inward current in hiPS-CMs. BTZ treatment reduced the I_{Na} current density, reaching statistical significance only at −20 mV (−38.5 ± 8.4 pA/pF Vs. −63.3 ± 19.1 pA/pF in untreated control cells), whereas no significance was observed at the other tested voltages. BTZ also induced a modest, non-significant rightward shift (~3.6 mV) in the voltage dependence of activation (Figure 5; Supplementary Table S4). In contrast, CFZ did not alter either the I_{Na} density or activation properties. The time course of inactivation was

10.3389/fddsv.2026.1774061

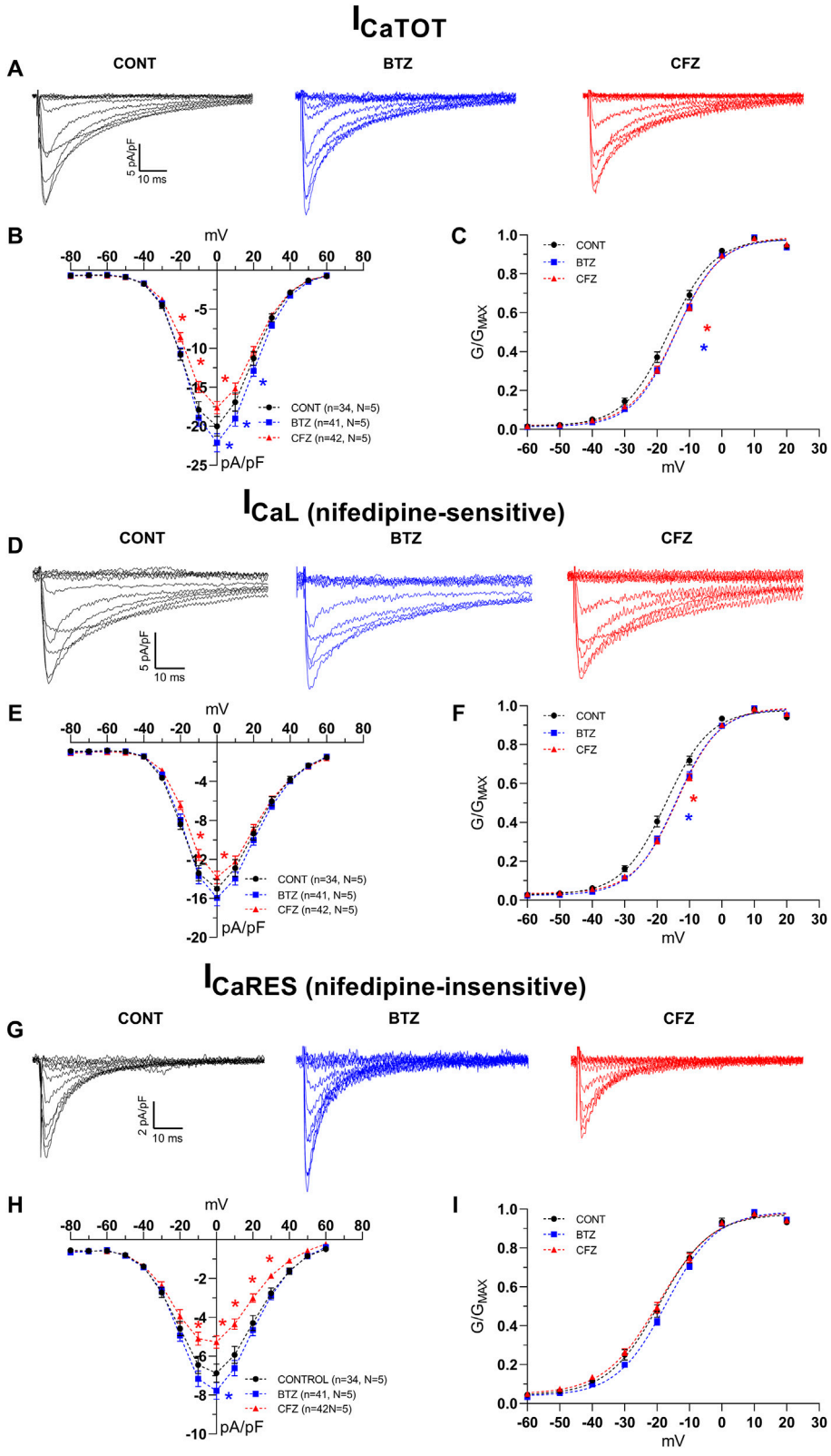

FIGURE 6
BTZ and CFZ effects on calcium currents in hiPS-CMs. **(A)** Representative I_{CaTOT} traces from control untreated cells (CONT) and from cells incubated with BTZ or CFZ. **(B)** Current-voltage relationship of I_{CaTOT} in control (black circles) and after the incubation with BTZ (blue squares) or CFZ (red triangles). **(C)** Voltage dependence of channel activation of I_{CaTOT} in control or after the incubation with BTZ and CFZ. **(D)** Representative nifedipine-sensitive I_{CaL} traces from control untreated cells (CONT) and from cells incubated with BTZ or CFZ. **(E)** Current voltage relationship of I_{CaL} in control (black circles) and after the incubation with BTZ (blue squares) or CFZ (red triangles). **(F)** Voltage dependence of channel activation of I_{CaL} in control or after the incubation with BTZ and CFZ. **(G)** Representative nifedipine-insensitive I_{CaRES} traces from control untreated cells (CONT) and from cells incubated with

(*Continued*)

FIGURE 6 (Continued)
BTZ or CFZ. **(H)** Current voltage relationship of I_{CaRES} in control (black circles) and after the incubation with BTZ (blue squares) or CFZ (red triangles). **(I)** Voltage dependence of channel activation of I_{CaRES} in control or after the incubation with BTZ and CFZ. (n = number of cells, N = number of differentiations) (*p < 0,05 2-Way ANOVA with Dunnet's *post hoc*).

unaffected by either compound (Supplementary Table S4). The effects of the two drugs were subsequently investigated on the total calcium current (I_{CaTOT}), the nifedipine-sensitive long-lasting component (I_{CaL}), and the residual nifedipine-insensitive component (Figure 6; Supplementary Table S4). The latter exhibited faster inactivation kinetics and a slightly more negative $V_{1/2}$ of activation respect to I_{CaTOT}, consistent with features previously described for T-type calcium channels (Perez-Reyes, 2003). However, because of its extremely small amplitude and the absence of a selective I_{CaT} inhibitor (Leuranguer et al., 2001), this component could not be pharmacologically isolated and was therefore designated as residual nifedipine-insensitive calcium current (I_{CaRES}) rather than I_{CaT}. BTZ treatment significantly increased I_{CaTOT} at membrane potentials between 0 and +20 mV, without affecting I_{CaL} density. A small but significant rightward shift in the voltage dependence of activation was observed for both the currents components (Supplementary Table S4). The increase in current density was also evident in the I_{CaRES}. In contrast, CFZ significantly reduced both I_{CaTOT} and I_{CaL} at voltages between −20 and 0 mV (Figure 6; Supplementary Table S4). Additionally, it induced a significant rightward shift (~3.1 mV) in the voltage dependence of I_{CaL} activation, whereas the corresponding shift in I_{CaTOT} (~1.9 mV) did not reach statistical significance. The inhibitory effect of CFZ was even more pronounced in the I_{CaRES}, particularly over the voltage range from −10 mV to +30 mV, suggesting a preferential effect on this calcium current activity.

3.5 Effects of BTZ and CFZ on potassium currents in hiPS-CMs

The effect of BTZ and CFZ on repolarizing currents were evaluated by measuring the total potassium current (I_{KTOT}, Figures 7A–C) and on the E-4031-sensitive component (I_{Kr}, Figures 7D–F). Neither compound significantly affected I_{KTOT} density, although both showed a trend toward reduction. In contrast, CFZ significantly decreased I_{Kr} density at +50 mV, whereas BTZ had no significant effect. No changes were observed in the voltage dependence of activation for either current component (Figure 7F; Supplementary Table S4). BTZ also appeared to slightly reduce the residual E-4031-insensitive potassium current component (data not shown). However, its very small amplitude and partial overlap with leak currents prevented a reliable quantitative characterization.

3.6 BTZ and CFZ do not alter the transcriptomic identity and maturation status of hiPSC-CMs

To determine whether the electrophysiological alterations induced by BTZ and CFZ were associated with transcriptional cardiotoxicity, dedifferentiation, or structural remodeling, the expression of key cardiac markers, maturation indices, and major ion channel genes was analyzed in treated hiPSC-CMs (Supplementary Figure S1; Supplementary Table S5). RT-PCR analysis showed that the expression of the structural marker *TNNT2* and the pan-cardiac transcription factor *NKX2.5* was unchanged following treatment, indicating the preservation of fundamental cardiac identity. Chamber specification and sarcomeric maturation were subsequently assessed through the analysis of atrial/fetal and ventricular/adult isoforms. Neither BTZ nor CFZ significantly perturbed the expression of fetal troponin I (*TNNI1*), adult troponin I (*TNNI3*), atrial myosin light chain 7 (*MYL7*), or ventricular myosin light chain 2 (*MYL2*). Crucially, the phenotypic ratios evaluating sarcomeric maturation (*TNNI3*/*TNNI1*) and ventricular specification (*MYL2*/*MYL7*) remained stable across all experimental conditions. Similar results were obtained for the adult-to-fetal *SCN5A* alternative splicing ratio (*SCN5A* adult/fetal). Potential transcriptional correlates of the electrophysiological alterations were further investigated by quantifying the expression of the ion channel genes analyzed in patch-clamp experiments. Transcript levels of *SCN5A* exon 25 (I_{Na}), *KCNH2* (I_{Kr}), *CACNA1C* (I_{CaL}), and *CACNA1H* (I_{CaT}) were unaffected by either treatments A trend toward reduced *SCN5A* expression and increased *CACNA1H* expression was observed in BTZ-treated cells, consistent with the decrease in I_{Na} current density and the increase in residual nifedipine-insensitive calcium current observed electrophysiologically (Figures 5, 6). Overall, these findings indicate that BTZ and CFZ, at the tested concentrations, do not impair the baseline transcriptomic profile, ion channel gene expression, or the maturation status of hiPSC-CMs.

4 Discussion

In this study, we investigated the chronic effects of clinically relevant nanomolar concentrations of the proteasome inhibitors bortezomib (BTZ) and carfilzomib (CFZ) on the electrophysiological properties of hiPS-CMs. Previous studies investigating PI-induced cardiotoxicity have predominantly relied on micromolar drug concentrations that induce overt cellular stress, mitochondrial dysfunction, and apoptosis. Under these conditions, both BTZ and CFZ have been shown to impair sarcomeric protein turnover, disrupt calcium handling, reduce contractile function in cardiomyocytes (Hasinoff et al., 2017), and altered autophagic signaling (Efentakis et al., 2019). Moreover, those models often reported greater toxicity for BTZ than CFZ, in contrast with clinical evidence. In actual clinical conditions, BTZ plasma concentration drops below 5 nM within 3 h after injection and CFZ has a half-life below 1 h, with a rapid plasma concentration decline observed within 15 min from the end of the injection (Moreau et al., 2012;

10.3389/fddsv.2026.1774061

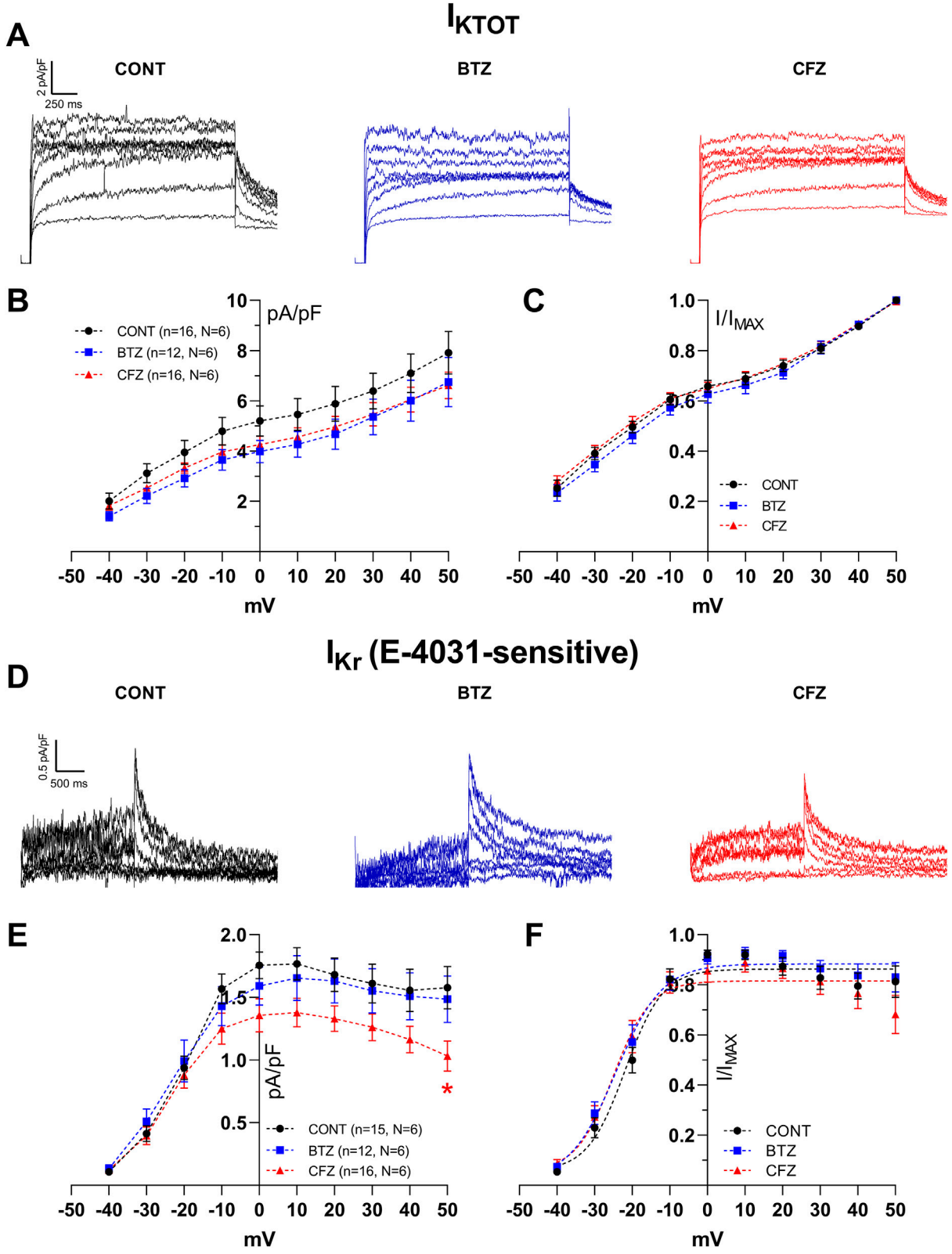

FIGURE 7
BTZ and CFZ effects on potassium currents in hiPS-CMs. **(A)** Representative I_{KTOT} traces from control untreated cells (CONT) and from cells incubated with BTZ or CFZ. **(B)** Current voltage relationship of I_{KTOT} in control (black circles) and after the incubation with BTZ (blue squares) or CFZ (red triangles). **(C)** Voltage dependence of channel activation of I_{KTOT} in control or after incubation with BTZ and CFZ. **(D)** Representative E-4031-sensitive I_{Kr} traces from control untreated cells (CONT) and from cells incubated with BTZ or CFZ. **(E)** Current voltage relationship of I_{Kr} in untreated cells (CONT, black circles) and after the incubation with BTZ (blue squares) or CFZ (red triangles). **(F)** Voltage dependence of channel activation of I_{Kr} in control or after the incubation with BTZ and CFZ. (n = number of cells, N = number of differentiations) (*$p < 0.05$ 2-Way ANOVA with Dunnet's *post hoc*).

Papadopoulos et al., 2013; Quach et al., 2017), making our experimental setting, which employs nanomolar concentrations, more closely aligned with the patient's chronic condition. *In vivo* studies have instead demonstrated acute CFZ-induced left ventricular dysfunction associated with cell damage and subsequent apoptosis, whereas BTZ produced minimal cardiac effects. While these studies identified plausible mechanisms involving ER stress, mitochondrial dysfunction, and metabolic remodeling (Nowis et al., 2010; Forghani et al., 2021; Tantawy et al., 2021), they do not fully explain the markedly different cardiotoxic profiles of BTZ and CFZ. By using nanomolar concentrations that induce substantial proteasomal inhibition without compromising cell viability, our experimental design allowed us to explore off-target or indirect effects on cardiac ion channel populations under conditions that more closely approximate chronic clinical exposure extending the current literature by identifying electrophysiological remodeling—occurring independently of overt cytotoxicity. At low nanomolar concentrations, BTZ exerted relatively mild effects on hiPS-CM electrophysiology. Regarding the parameters describing spontaneous action potentials, it did not significantly affect the maximum diastolic potential, firing frequency, or action potential amplitude. However, a non-significant trend toward a reduced upstroke velocity (dV/dt) and a prolongation of the repolarization phase was observed. With regard of the stimulated activity, BTZ did not significantly affect any of the considered parameters, confirming its overall milder effect on hiPS-CMs electrophysiology. At the ionic current level, BTZ induced a reduction in sodium current density, similarly to what is reported for other sodium channel isoforms in mice DRGs (Zhou et al., 2023). This observation is consistent with the observed decrease in dV/dt and with the non-significant decrease in *SCN5A* transcription. Moreover, data highlight an increase in the nifedipine-insensitive component of the calcium current, confirmed by a similar trend in *CACNA1H* transcription and consistent with previous reports of BTZ-induced upregulation of Cav3.2 channels in other excitable cell types (Tomita et al., 2019). Because this calcium current component is active within a voltage range between −10 and +10 mV, it may contribute to the tendency toward action potential prolongation. The preservation of action potential amplitude despite the reduction in sodium current may be explained by the fact that, in our model, inward currents activate within the same voltage range (−40 to −30 mV), with functional compensation between the decreased sodium current and the increased calcium current. In contrast, the reduced dV/dt more directly reflects the decrease in sodium current, consistent with its dominant role in the rapid depolarization phase. In addition, BTZ treated cells displayed a slight reduction in total potassium outward current which could further favor prolongation of the action potential duration. In particular, no significant alteration was found in I_{Kr}, implying a reduction of potassium conductance other than that, barely measurable. Importantly, BTZ treatment did not severely modify the distribution of hiPS-CM electrophysiological profile subtypes, which remained comparable to that of untreated cells and predominantly ventricular-like for both spontaneous and triggered APs. Together, these findings indicate that BTZ-induced electrophysiological changes are limited in magnitude and partially compensated by opposing ionic mechanisms, consistent with its relatively favorable cardiac safety profile observed clinically. In contrast, CFZ profoundly altered cardiomyocyte electrophysiology even at similarly low nanomolar concentrations. Regarding the parameters describing spontaneous action potentials, CFZ treatment induced a significant depolarization of the maximum diastolic potential, without affecting firing frequency, while reducing action potential amplitude. Analysis of repolarization duration revealed a tendency toward shortening of the early phases (APD30 and APD50), accompanied by prolongation of the late phases (APD70 and APD90), as further supported by changes in the APD50/APD90 ratio, indicative of selective repolarization remodeling. In addition, CFZ significantly reduced the action potential upstroke velocity. Regarding the stimulated action potentials, CFZ reduced all the calculated APDs and slightly increased the dV/dt without reaching statistical significance. This partial discrepancy with the spontaneous APs data could be explained by the imposition of a hyperpolarized resting membrane potential required to effectively trigger a stimulated response. This may have masked the depolarizing effect of CFZ, leading to different ion channels availability between spontaneous and triggered APs. Overall, the more relevant observation should be the general alteration of hiPS-CMs electrophysiology by CFZ. At the level of ionic currents, CFZ did not substantially alter inward sodium current, except for a slight trend toward a depolarizing shift in the activation curve. In contrast, it induced a reduction in inward calcium current, which was more pronounced for the nifedipine-insensitive component than for the L-type current. Since T-type calcium channels are known to contribute to the upstroke phase of pacemaker action potentials (Hagiwara et al., 1988), the effect of CFZ on the nifedipine-insensitive calcium current may underline the dV/dt reduction observed on spontaneous APs. The differential effect observed on the dV/dt in triggered APs might be a consequence of the artificially imposed hyperpolarized resting membrane potential that may have altered the availability of sodium and calcium currents. Finally, CFZ significantly reduced the density of the rapid delayed rectifier potassium current (I_{Kr}) that aligns with previous observations of CFZ-induced inhibition of delayed rectifier potassium in other excitable cell models (So et al., 2019). Taken together, these changes suggest that, within the dynamic process of action potential generation, the reduction in dV/dt may be explained by a fraction of sodium channels that, in the presence of a more depolarized MDP, remain trapped in the inactivated state. The decrease in action potential amplitude can be interpreted not only as a consequence of reduced sodium channel availability but also considering the concomitant reduction in calcium current. Similarly, the reduction in outward potassium currents provides a plausible explanation for the prolongation of the late repolarization phase. This global electrophysiological remodeling supports the emergence and predominance of a cellular population that, based on action potential characteristics, can be classified as nodal-like, at the expense of ventricular-like and, to a lesser extent, atrial-like populations. This subpopulation profile distribution is not considered physiological, since the electrophysiological maturation of hiPSCs typically evolves toward a more ventricular-like phenotype over time (Barbuti et al., 2016). The presence of cells with nodal-like AP profile may lead to ectopic automaticity or

triggered activity, and the unbalance fluxes of sodium and calcium current may be related to arrhythmia (Mesirca et al., 2015; Veerman et al., 2015). Interestingly, the alterations on the electrophysiological profile and subpopulations distribution were not reflected at the transcriptional level since all the markers tested to detect eventual dedifferentiation and structural alteration were unaffected in all the tested conditions. Thus, CFZ seems not to cause a "true" cellular remodeling of hiPS-CMs. The molecular basis behind its stronger effects may rely on mechanisms other than gene expression regulation and remain to be unraveled.

Altogether, our findings indicate a previously unrecognized subclinical electrophysiological remodeling induced by CFZ, which could contribute to a cellular substrate more permissive to arrhythmogenic events. While the present data do not allow direct inference of specific clinical arrhythmias, they are consistent with the more pronounced cardiac safety concerns reported for CFZ compared with BTZ. Clinically, CFZ has been associated with supraventricular and ventricular arrhythmic events, whereas BTZ has only rarely been linked to arrhythmias (Atrash et al., 2015; El-Cheikh et al., 2023). In line with this differential clinical profile, recent analyses of the FDA Adverse Event Reporting System have identified QTc prolongation and torsade de pointes as emerging safety signals for CFZ (Buck et al., 2022). Since drug-induced torsade de pointes is commonly associated with QTc prolongation and hERG/I_{Kr} inhibition (Hancox et al., 2008), the CFZ-dependent reduction in I_{Kr} density observed in hiPSC-CMs may represent a mechanistic finding of potential relevance. However, this interpretation should be considered cautiously, as our experimental model does not directly reproduce the complexity of patient-level arrhythmic outcomes. Conversely, BTZ produced more limited electrophysiological changes in our model and has only rarely been associated with QTc interval prolongation, often in combination with other chemotherapeutic agents, with no torsade de pointes events reported so far (Lü et al., 2009; Walker et al., 2013; Duan et al., 2018). In conclusion, this study confirms the higher cardiotoxic potential of CFZ compared with BTZ and identifies perturbation in cardiac electrophysiology as a previously underappreciated mechanism of PI-induced cardiotoxicity. Importantly, these effects occurred in the absence of overt cytotoxicity, indicating that electrophysiological dysfunction may represent an early and independent contributor to PI-associated cardiovascular risk. These findings underscore the need for heightened cardiovascular vigilance when prescribing CFZ, particularly in patients with pre-existing cardiac risk factors or those receiving concomitant cardioactive medications. Although BTZ displays a more favorable cardiac safety profile, its ability to modulate cardiac ion channel populations suggests that caution remains warranted, especially in combination therapies that may synergistically increase the risk of adverse cardiovascular events.

5 Study limitations

Several limitations should be acknowledged. As with all studies based on hiPSC-derived cardiomyocytes, the intrinsic immaturity of the model remains a major constraint when interpreting electrophysiological phenotypes and extrapolating the findings to the adult myocardium. This is particularly relevant for parameters such as maximum diastolic potential and action potential upstroke velocity, which are strongly influenced by the maturation state of hiPSC-CMs. The use of more advanced maturation strategies in future studies may improve the physiological relevance of this experimental model.

The study was also performed using a single female hiPSC line; therefore, possible sex-related effects and line-to-line variability could not be assessed. In addition, all conclusions are based on a single nanomolar concentration and a single exposure time for each drug. Although these experimental conditions were clinically motivated, additional dose-response and time-course studies would be needed to determine whether the observed electrophysiological alterations represent early adaptive responses or more advanced remodeling processes. Moreover, the present study does not formally establish a direct mechanistic link between proteasome inhibition and the electrophysiological changes induced by CFZ.

For the sake of signal stability and overall data quality, spontaneous action potentials were recorded from small clusters of cells. In this setting, potential effects of BTZ and CFZ on intercellular coupling cannot be fully excluded. Although formal beat-to-beat variability analysis was not performed, the relatively low variability observed within individual recordings suggested an overall stable spontaneous firing behavior under our experimental conditions. Nevertheless, future assessment of conduction velocity and propagation dynamics would further strengthen the interpretation of the observed action potential and ionic current alterations, particularly in relation to intercellular coupling and arrhythmogenic susceptibility at the multicellular level.

Another limitation is related to the heterogeneous nature of the hiPSC-CM population. In this initial study, established methods to enrich or segregate atrial- and ventricular-like subpopulations were not applied; therefore, experiments were performed on mixed cardiomyocyte preparation. Consequently, the classification of cells as nodal-, atrial-, or ventricular-like was performed *a posteriori*. The observed changes may therefore reflect increased electrophysiological heterogeneity rather than a definitive shift in cardiomyocyte lineage identity. This aspect may also have led to an underestimation of drug-induced differences at the level of transmembrane ionic currents.

Furthermore, action potential recordings and ionic current measurements were obtained from different cell populations because of the distinct experimental conditions required. Specifically, action potentials were recorded from small cell clusters, whereas ionic currents were measured at the single-cell level, often using different recording solutions. In addition, as indicated by the scales shown in the figures, some ionic currents were very small in amplitude, limiting the reliability of quantitative analysis. Finally, despite the drug-induced impairment in calcium current, intracellular calcium handling was not investigated in the present work and will require further dedicated studies to better define the functional consequences of BTZ and CFZ exposure.

Data availability statement

The raw data supporting the conclusions of this article will be made available by the authors, without undue reservation.

Ethics statement

Ethical approval was not required for the studies on humans in accordance with the local legislation and institutional requirements because only commercially available established cell lines were used.

Author contributions

DM: Conceptualization, Data curation, Formal Analysis, Methodology, Writing – original draft, Writing – review and editing. SC: Methodology, Writing – original draft. AF: Data curation, Formal Analysis, Writing – original draft. RP: Methodology, Writing – original draft. AM: Methodology, Writing – original draft. LA: Funding acquisition, Writing – review and editing. CP: Funding acquisition, Writing – review and editing. GN: Supervision, Writing – review and editing. GC: Supervision, Writing – review and editing. IR: Conceptualization, Resources, Supervision, Writing – original draft, Writing – review and editing.

Funding

The author(s) declared that financial support was received for this work and/or its publication. This project is supported by grant from Ministero dell'Università e della Ricerca-NextGenerationEU (PNRR M4.C2.I1.1- Avviso 104/2022, CUP H53D23006370006 Project title "A study investigating post-translational modifications in Brugada Syndrome and their effects on cardiac activity using hIPSC-derived cardiomyocytes", from University of Milano-Bicocca (Fondo Ateneo per la Ricerca 2024-ATE-0119) and from the Ricerca Corrente funding provided by the Italian Ministry of Health to IRCCS Policlinico San Donato and by IRCCS Policlinico San Donato own funds.

Conflict of interest

The author(s) declared that this work was conducted in the absence of any commercial or financial relationships that could be construed as a potential conflict of interest.

The authors GC, LA declared that they were an editorial board member of Frontiers at the time of submission. This had no impact on the peer review process and the final decision.

Generative AI statement

The author(s) declared that generative AI was used in the creation of this manuscript. To help edit the manuscript and the Generative AI is not listed as an author of the manuscript. The use of Generative AI has been included in the acknowledgements section of the manuscript, listing the name and source of the Generative AI.

Any alternative text (alt text) provided alongside figures in this article has been generated by Frontiers with the support of artificial intelligence and reasonable efforts have been made to ensure accuracy, including review by the authors wherever possible. If you identify any issues, please contact us.

Publisher's note

Supplementary material

The Supplementary Material for this article can be found online at: https://www.frontiersin.org/articles/10.3389/fddsv.2026.1774061/full#supplementary-material

References

Atrash, S., Tullos, A., Panozzo, S., Bhutani, M., Van Rhee, F., Barlogie, B., et al. (2015). Cardiac complications in relapsed and refractory multiple myeloma patients treated with carfilzomib. *Blood Cancer J.* 5 (1), e272. doi:10.1038/bcj.2014.93

Barbuti, A., Benzoni, P., Campostrini, G., and Dell'Era, P. (2016). Human derived cardiomyocytes: a decade of knowledge after the discovery of induced pluripotent stem cells. *Dev. Dynamics* 245 (12), 1145–1158. doi:10.1002/dvdy.24455

Buck, B., Kellett, E., Addison, D., and Vallakati, A. (2022). Carfilzomib-induced cardiotoxicity: an analysis of the FDA adverse event reporting system (FAERS). *J. Saudi Heart Assoc.* 34 (3), 134–141. doi:10.37616/2212-5043.1311

Burridge, P. W., Matsa, E., Shukla, P., Lin, Z. C., Churko, J. M., Ebert, A. D., et al. (2014). Chemically defined generation of human cardiomyocytes. *Nat. Methods* 11 (8), 855–860. doi:10.1038/nmeth.2999

Buza, V., Rajagopalan, B., and Curtis, A. B. (2017). Cancer treatment-induced arrhythmias: focus on chemotherapy and targeted therapies. *Circulation* 10 (8), e005443. doi:10.1161/CIRCEP.117.005443

Calamaio, S., Serzanti, M., Boniotti, J., Fra, A., Garrafa, E., Cominelli, M., et al. (2023). Human iPSC-Derived 3D hepatic organoids in a miniaturized dynamic culture system. *Biomedicines* 11 (8), 2114. doi:10.3390/biomedicines11082114

Caller, T., Moore, K. J., Lehmann, L. H., Wu, S. M., and Leor, J. (2025). Insights into heart-tumor interactions in heart failure. *Circulation Research* 136 (11), 1262–1285. doi:10.1161/CIRCRESAHA.124.325490

Cammann, C., Kulla, J., Wiebusch, L., Walz, C., Zhao, F., Lowinus, T., et al. (2023). Proteasome inhibition potentiates Kv1.3 potassium channel expression as therapeutic target in drug-sensitive and -resistant human melanoma cells. *Biomed. Pharm.* 168, 115635. doi:10.1016/j.biopha.2023.115635

Chen, J. H., Lenihan, D. J., Phillips, S. E., Harrell, S. L., and Cornell, R. F. (2017). Cardiac events during treatment with proteasome inhibitor therapy for multiple myeloma. *Cardio-oncology Lond. Engl.* 3, 4. doi:10.1186/s40959-017-0023-9

Dimopoulos, M. A., Moreau, P., Palumbo, A., Joshua, D., Pour, L., Hájek, R., et al. (2016). Carfilzomib and dexamethasone versus bortezomib and dexamethasone for patients with relapsed or refractory multiple myeloma (ENDEAVOR): a randomised, phase 3, open-label, multicentre study. *Lancet. Oncol.* 17 (1), 27–38. doi:10.1016/S1470-2045(15)00464-7

Diwadkar, S., Patel, A. A., and Fradley, M. G. (2016). Bortezomib-induced complete heart block and myocardial scar: the potential role of cardiac biomarkers in monitoring cardiotoxicity. *Case Reports Cardiology* 2016, 3456287. doi:10.1155/2016/3456287

Duan, J., Tao, J., Zhai, M., Li, C., Zhou, N., Lv, J., et al. (2018). Anticancer drugs-related QTc prolongation, torsade de pointes and sudden death: current evidence and future research perspectives. *Oncotarget* 9 (39), 25738–25749. doi:10.18632/oncotarget.25008

Efentakis, P., Kremastiotis, G., Varela, A., Nikolaou, P. E., Papanagnou, E. D., Davos, C. H., et al. (2019). Molecular mechanisms of carfilzomib-induced cardiotoxicity in mice and the emerging cardioprotective role of metformin. *Blood* 133 (7), 710–723. doi:10.1182/blood-2018-06-858415

El-Cheikh, J., Moukalled, N., Malard, F., Bazarbachi, A., and Mohty, M. (2023). Cardiac toxicities in multiple myeloma: an updated and a deeper look into the effect of different medications and novel therapies. *Blood Cancer J.* 13 (1), 83. doi:10.1038/s41408-023-00849-z

Forghani, P., Rashid, A., Sun, F., Liu, R., Li, D., Lee, M. R., et al. (2021). Carfilzomib treatment causes molecular and functional alterations of human induced pluripotent stem cell-derived cardiomyocytes. *J. Am. Heart Assoc.* 10 (24), e022247. doi:10.1161/JAHA.121.022247

GBD 2017 Causes of Death Collaborators (2018). Global, regional, and national age-sex-specific mortality for 282 causes of death in 195 countries and territories, 1980-2017: a systematic analysis for the global burden of disease study 2017. *Lancet* 392 (10159), 1736–1788. doi:10.1016/S0140-6736(18)32203-7

Georgiopoulos, G., Makris, N., Laina, A., Theodorakakou, F., Briasoulis, A., Trougakos, I. P., et al. (2023). Cardiovascular toxicity of proteasome inhibitors: underlying mechanisms and management strategies: *JACC: cardiooncology* State-of-the-Art review. *JACC. CardioOncology* 5 (1), 1–21. doi:10.1016/j.jaccao.2022.12.005

Hagiwara, N., Irisawa, H., and Kameyama, M. (1988). Contribution of two types of calcium currents to the pacemaker potentials of rabbit sino-atrial node cells. *J. Physiology* 395, 233–253. doi:10.1113/jphysiol.1988.sp016916

Hancox, J. C., McPate, M. J., El Harchi, A., and Zhang, Y. H. (2008). The hERG potassium channel and hERG screening for drug-induced torsades de pointes. *Pharmacol. Therapeutics* 119 (2), 118–132. doi:10.1016/j.pharmthera.2008.05.009

Hasinoff, B. B., Patel, D., and Wu, X. (2017). Molecular mechanisms of the cardiotoxicity of the proteasomal-targeted drugs Bortezomib and Carfilzomib. *Cardiovasc. Toxicology* 17 (3), 237–250. doi:10.1007/s12012-016-9378-7

Ito, S. (2020). Proteasome inhibitors for the treatment of multiple myeloma. *Cancers* 12 (2), 265. doi:10.3390/cancers12020265

Koivumäki, J. T., Naumenko, N., Tuomainen, T., Takalo, J., Oksanen, M., Puttonen, K. A., et al. (2018). Structural immaturity of human iPSC-Derived cardiomyocytes: *in silico* investigation of effects on function and disease modeling. *Front. Physiology* 9, 80. doi:10.3389/fphys.2018.00080

Kortuem, K. M., and Stewart, A. K. (2013). Carfilzomib. *Blood* 121 (6), 893–897. doi:10.1182/blood-2012-10-459883

Leuranguer, V., Mangoni, M. E., Nargeot, J., and Richard, S. (2001). Inhibition of T-type and L-type calcium channels by mibefradil: physiologic and pharmacologic bases of cardiovascular effects. *J. Cardiovascular Pharm.* 37 (6), 649–661. doi:10.1097/00005344-200106000-00002

Lü, S., Wang, J., Xu, X., Ni, X., Huang, C., Qiu, H., et al. (2009). Bortezomib in combination with epirubicin, dexamethasone and thalidomide is a highly effective regimen in the treatment of multiple myeloma: a single-center experience. *Int. Journal Hematology* 89 (1), 34–38. doi:10.1007/s12185-008-0218-9

Ma, J., Guo, L., Fiene, S. J., Anson, B. D., Thomson, J. A., Kamp, T. J., et al. (2011). High purity human-induced pluripotent stem cell-derived cardiomyocytes: electrophysiological properties of action potentials and ionic currents. *Am. Journal Physiology* 301 (5), H2006–H2017. doi:10.1152/ajpheart.00694.2011

Malacrida, A., Semperboni, S., Di Domizio, A., Palmioli, A., Broggi, L., Airoldi, C., et al. (2021). Tubulin binding potentially clears up Bortezomib and Carfilzomib differential neurotoxic effect. *Sci. Reports* 11 (1), 10523. doi:10.1038/s41598-021-89856-3

Meijers, W. C., Aboumsallem, J. P., Lyon, A. R., Moslehi, J., and de Boer, R. A. (2026). Forward and reverse cardio-oncology. *Physiol. Reviews* 106 (1), 587–644. doi:10.1152/physrev.00041.2024

Mesirca, P., Torrente, A. G., and Mangoni, M. E. (2015). Functional role of voltage gated Ca(2+) channels in heart automaticity. *Front. Physiology* 6, 19. doi:10.3389/fphys.2015.00019

Moreau, P., Karamanesht, I. I., Domnikova, N., Kyselyova, M. Y., Vilchevska, K. V., Doronin, V. A., et al. (2012). Pharmacokinetic, pharmacodynamic and covariate analysis of subcutaneous versus intravenous administration of bortezomib in patients with relapsed multiple myeloma. *Clin. Pharmacokinetics* 51 (12), 823–829. doi:10.1007/s40262-012-0010-0

Nowis, D., Maczewski, M., Mackiewicz, U., Kujawa, M., Ratajska, A., Wieckowski, M. R., et al. (2010). Cardiotoxicity of the anticancer therapeutic agent bortezomib. *Am. Journal Pathology* 176 (6), 2658–2668. doi:10.2353/ajpath.2010.090690

Papadopoulos, K. P., Burris, H. A., Gordon, M., Lee, P., Sausville, E. A., Rosen, P. J., et al. (2013). A phase I/II study of carfilzomib 2-10-min infusion in patients with advanced solid tumors. *Cancer Chemotherapy Pharmacology* 72 (4), 861–868. doi:10.1007/s00280-013-2267-x

Perez-Reyes, E. (2003). Molecular physiology of low-voltage-activated t-type calcium channels. *Physiol. Reviews* 83 (1), 117–161. doi:10.1152/physrev.00018.2002

Quach, H., White, D., Spencer, A., Ho, P. J., Bhutani, D., White, M., et al. (2017). Pharmacokinetics and safety of carfilzomib in patients with relapsed multiple myeloma and end-stage renal disease (ESRD): an open-label, single-arm, phase I study. *Cancer Chemotherapy Pharmacology* 79 (6), 1067–1076. doi:10.1007/s00280-017-3287-8

Schlafer, D., Shah, K. S., Panjic, E. H., and Lonial, S. (2017). Safety of proteasome inhibitors for treatment of multiple myeloma. *Expert Opinion Drug Safety* 16 (2), 167–183. doi:10.1080/14740338.2017.1259310

Siegel, D., Martin, T., Nooka, A., Harvey, R. D., Vij, R., Niesvizky, R., et al. (2013). Integrated safety profile of single-agent carfilzomib: experience from 526 patients enrolled in 4 phase II clinical studies. *Haematologica* 98 (11), 1753–1761. doi:10.3324/haematol.2013.089334

So, E. C., Liu, P. Y., Lee, C. C., and Wu, S. N. (2019). High effectiveness in actions of Carfilzomib on delayed-rectifier K^+ Current and on spontaneous action potentials. *Front. Pharmacology* 10, 1163. doi:10.3389/fphar.2019.01163

Stewart, A. K., Rajkumar, S. V., Dimopoulos, M. A., Masszi, T., Špička, I., Oriol, A., et al. (2015). Carfilzomib, lenalidomide, and dexamethasone for relapsed multiple myeloma. *N. Engl. Journal Medicine* 372 (2), 142–152. doi:10.1056/NEJMoa1411321

Tantawy, M., Chekka, L. M., Huang, Y., Garrett, T. J., Singh, S., Shah, C. P., et al. (2021). Lactate dehydrogenase B and pyruvate oxidation pathway associated with Carfilzomib-Related cardiotoxicity in multiple myeloma patients: result of a multi-omics integrative analysis. *Front. Cardiovascular Medicine* 8, 645122. doi:10.3389/fcvm.2021.645122

Tarantino, A., Ciconte, G., Melgari, D., Frosio, A., Ghiroldi, A., Piccoli, M., et al. (2024). NaV1.5 autoantibodies in Brugada syndrome: pathogenetic implications. *Eur. Heart Journal* 45 (40), 4336–4348. doi:10.1093/eurheartj/ehae480

Tomita, S., Sekiguchi, F., Deguchi, T., Miyazaki, T., Ikeda, Y., Tsubota, M., et al. (2019). Critical role of $Ca_v3.2$ T-type calcium channels in the peripheral neuropathy induced by bortezomib, a proteasome-inhibiting chemotherapeutic agent, in mice. *Toxicology* 413, 33–39. doi:10.1016/j.tox.2018.12.003

Veerman, C. C., Wilde, A. A., and Lodder, E. M. (2015). The cardiac sodium channel gene SCN5A and its gene product NaV1.5: role in physiology and pathophysiology. *Gene* 573 (2), 177–187. doi:10.1016/j.gene.2015.08.062

Walker, A. R., Klisovic, R., Johnston, J. S., Jiang, Y., Geyer, S., Kefauver, C., et al. (2013). Pharmacokinetics and dose escalation of the heat shock protein inhibitor 17-allyamino-17-demethoxygeldanamycin in combination with bortezomib in relapsed or refractory acute myeloid leukemia. *Leukemia and Lymphoma* 54 (9), 1996–2002. doi:10.3109/10428194.2012.760733

Wu, P., Oren, O., Gertz, M. A., and Yang, E. H. (2020). Proteasome inhibitor-related cardiotoxicity: mechanisms, diagnosis, and management. *Curr. Oncology Reports* 22 (7), 66. doi:10.1007/s11912-020-00931-w

Zhou, Z., Nagayasu, K., Shirakawa, H., and Kaneko, S. (2023). Specific cellular effects of low bortezomib concentrations on purified cultures of Schwann cells, satellite glial cells, macrophages, and dorsal root ganglion neurons. *Biol. Pharmaceutical Bulletin* 46 (1), 102–110. doi:10.1248/bpb.b22-00668